Astron. Astrophys. 325, 450–456 (1997)

ASTRONOMY
AND
ASTROPHYSICS

Origin of the IR continuum in the Circinus galaxy⋆

Ralf Siebenmorgen[1], **Alan Moorwood**[2], **Wolfram Freudling**[2,3], **and Hans Ulrich Käufl**[2]

[1] ISO Science Operations Centre, Astrophysics Division of ESA, Villafranca del Castillo, P.O. Box 50727, E-28080 Madrid, Spain
[2] European Southern Observatory, Karl-Schwarzschild-Str. 2, D-85748 Garching bei München, Germany
[3] Space Telescope – European Coordinating Facility, Karl-Schwarzschild-Str. 2, D-85748 Garching bei München, Germany

Received 21 October 1996 / Accepted 7 March 1997

Abstract. We present infrared and millimeter–wave observations of the Circinus galaxy which is at a distance of only 4 Mpc and provides the closest example of an obscured Seyfert nucleus surrounded by a starburst ring. The FWHM size of the continuum emission is found to be only $\simeq$ 0.3" (6pc) at 3-5 μm, $\simeq$ 1.3" at 10μm, $\leq$ 1.5" at 20μm and $\leq$ 23" (460pc) at 1.3 mm. The 1.3 mm measurements also provide an estimate of $\simeq 1.6 \cdot 10^8 M_\odot$ for the gas mass. It is shown using a radiative transfer code that both the observed sizes and overall spectral energy distribution, including the 9.7μm silicate absorption and 3.28 - 11.3 μm PAH emission features, can be satisfactorily modelled by assuming that the total luminosity is dominated by dust heated by a central power law source.

Key words: galaxies: individual: Circinus – infrared: galaxies – Infrared: ISM: continuum – dust, extinction

1. Introduction

The Circinus galaxy (A1409-65) is a large ($\simeq$ 17') spiral of type S(b-d) at a distance $\simeq$ 4 Mpc which is located in a region of low extinction close to the galactic plane (Freeman et al., 1977). It is of particular interest as the closest example of a galaxy containing an obscured Seyfert nucleus surrounded by circumnuclear starburst activity. Evidence for the Seyfert activity is provided by its spectacular ionization cone (Marconi et al., 1994); prominent high excitation coronal line spectrum (Oliva et al., 1994; Moorwood et al., 1996, hereafter M96) and hard X-ray continuum (Matt et al., 1996). Star formation activity traced by Hα (Marconi et al., 1994) and Brγ recombination line emission (Moorwood & Oliva, 1994) peaks in a partial ring of radius $\simeq$ 200pc. Based on the nuclear continuum deduced from its emission line spectrum and the ionization rate inferred for the starburst ring, Moorwood et al. (1996) have suggested that the starburst may contribute only $\simeq$10% of the total luminosity rather than the $\simeq$ 70% inferred previously by Rowan-Robinson & Crawford (1989) from a decomposition of its spectral energy distribution in the IRAS bands. Nevertheless, pronounced PAH features, normally associated with the presence of hot stars, are seen from the ground at 3.28μm within a 7.5" aperture (Moorwood, 1986) and at 6.2, 7.7, 8.8 and 11.3μm within a 14 x 20" aperture with ISO (M96). Both the ground-based and ISO spectra also show pronounced 9.7μm silicate absorption. The overall infrared 1.2 - 100μm spectral energy distribution based on ground-based and IRAS observations has been published by Moorwood & Glass (1984) and the recently obtained 2.5 - 45μm spectrum obtained with ISO appears in M96.

In this paper we present measurements of the size of the infrared and millimeter emitting region and test, using the radiative transfer code developed by Krügel & Siebenmorgen (1994, hereafter KS94), if the size versus wavelength; overall spectral energy distribution and presence of PAH features can be modelled assuming that the dust heating is dominated by a central power law source.

2. Observations

2.1. 1.3mm continuum emission

Continuum emission at 1.3 mm was detected with the 15m ESO/Swedish SEST telescope at La Silla during the nights of 10/11 July 1993 at the nominal galaxy center coordinates of 14h09m17.9, -65 ^{o}06'18". The observations were performed with the MPIfR bolometer detector (Kreysa, 1990) in chopping and beam switching mode with a beam separation of 70". Uranus was used as the calibration standard assuming a brightness temperature of 101K and was mapped to determine both the beam shape and the sensitivity of the bolometer. The beam is Gaussian but elongated in elevation. The measured mean aperture was $23'' \pm 1''$ at full width half maximum (FWHM). The atmospheric transmission was determined by sky dips every 30 minutes. Zenith opacities were $0.13 \leq \tau_{1.3} \leq 0.2$. Pointing and focus checks were performed typically once per hour. The focus was stable nearly the whole night and the pointing accuracy varied by less than 4" in azimuth and 6" in elevation. As a pointing reference source we have used the Quasar 1424-418. Individual

Send offprint requests to: rsiebenm@iso.vilspa.esa.es

⋆ Based on observations collected at the European Southern Observatory, La Silla, Chile (ESO 53.1-069, 53.1-051)

Table 1. The 1.3mm continuum emission of Circinus

position	$\Delta\alpha$ ”	$\Delta\delta$ ”	time sec	F mJy	σ
center	0	0	2160	222.3 ± 7	31
pos 1	+21.6	+24.9	360	< 94	3
pos 2	+21.6	-24.9	3240	< 20	3
pos 3	-21.6	+24.9	720	< 51	3
pos 4	-21.6	-24.9	2160	< 40	3
Σ pos			6480	< 17	3

ON–OFF pairs consisted of 10 cycles with 12 sec integration time each.

As cold dust halos have been detected around the star-burst galaxies M82 and N253 (Krügel et al. 1990, Chini et al., 1992a, Hughes et al., 1994) we also searched for a similar halo around Circinus by observing at positions offset by one beam-size ($\approx 23''$) from the center position of the galaxy. The results are summarized in Table 1. There is a clear detection at the center but nothing to a limit of 3σ at any of the offset positions.

The atmospheric conditions during the first night were sufficiently stable to obtain a 4’ $\times$ 3’ map of the 1.3mm continuum emission. The map was centered at the central position of the beam switching observations. A scan velocity of 8”/sec in azimuth and scan separation of 8” was used. Each scan was measured with a beam throw of 70” in azimuth. A total of 16 individual maps were obtained in 3 hours 20 minutes. Observations of the center position in beam switching mode were made after each pointing to check both the focus and tracking. The data have been analyzed using the SEST software package. Fig. 1 shows the final map in which individual exposures have been convolved into a single beam image in which sky noise and chopping effects have been corrected.

Comparison with a map of Uranus shows that Circinus is unresolved and gives a mean calibration factor of 2.4 mJy/count yielding a peak flux of 248 ± 46.1 mJy ($5.4\ \sigma$) which is in agreement with the ON – OFF detection.

2.2. 3-5μm imaging

Previously unpublished one dimensional speckle interferometry in the L’(3.8μm) and M(4.8μm) bands was performed at the ESO 3.6m telescope in 1987 using the instrument described by Perrier(1986) together with scanning of the telescope secondary mirror to produce diffraction limited slit scans at PA 90^o. The raw scans both have FWHM $\simeq$ 0.3” corresponding to the telescope diffraction limit at 5μm. More detailed analysis of the L band visibility curve shows that it can be well fitted by a source emitting 80% of its energy within a 0.3” (FWHM) core and the rest in an extended halo. This is also consistent with the M band

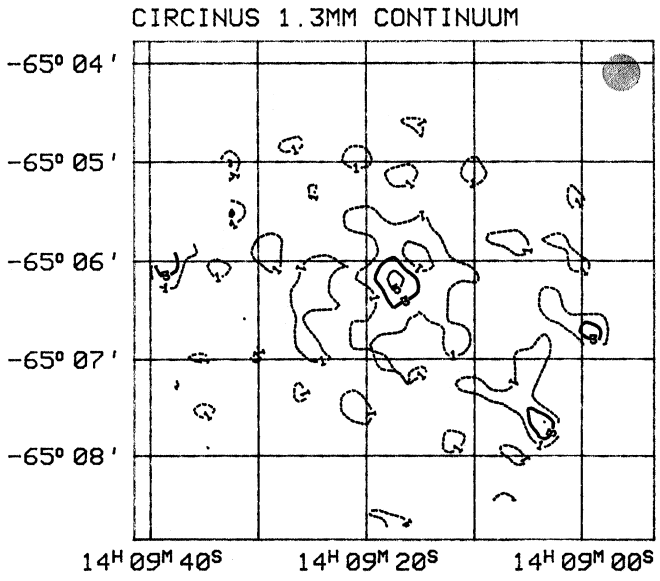

Fig. 1. 1.3mm continuum map of the S(b-d) Circinus galaxy. The 1σ (= 46mJy), 3σ and 5σ contours are plotted. The beam is shown as the hashed area in the upper right corner.

data, although fits to the visibility in this case are less reliable due to the lower s/n ratio. As the speckle observations were restricted to scan lengths of 6” they are insensitive to larger scale components e.g. starlight. A subsequent direct L band image obtained with the IRAC1 array camera at the ESO 2.2m telescope confirms that most of the energy is confined to a central spike although the FWHM in this case was seeing limited at 0.7”.

2.3. Mid IR imaging

A first attempt to determine the extent of the mid-infrared emission was made by one of us (AM) at the ESO 3.6m telescope in 1987 by performing N(10μm) and Q(20μm) band linear scans with a 1.5” slit. In both cases the profiles are indistinguishable from those obtained for a reference star and show the diffraction rings at 20μm.

Direct images around 10μm were made on May 21/22 1994 with the Thermal Infrared Multimode Instrument (TIMMI) mounted at ESO’s 3.6m telescope (Käufl et al., 1994). TIMMI is a cryogenic focal reducer equipped with a 64x64 element Si:Ga detector. We used for the observations the following filters:

- standard N–filter (λ_{center} = 9.3μm, $\Delta\lambda$ = 5μm)
- narrow band filter centered around the 11.3 μm PAH transition (λ_{center} = 11.18μm, $\Delta\lambda$ = 0.44μm)
- narrow band filter centered around the 8.6 μm PAH transition (λ_{center} = 8.51μm, $\Delta\lambda$ = 0.31μm)

The scale of the images obtained is 0.34 ”/pixel and the total field of view $\approx 20 \times 20$ arcsec^2. In order to determine the point spread function, we also imaged the stars αCen and βGru. The size of the point spread function was determined by a two dimensional Gaussian fit to be 1.2×1.5 arcsec^2.

As the observing nights were not photometric the images have been calibrated photometrically using the aperture photometry obtained by Moorwood & Glass (1984) by simulating their apertures on the images. The flux as a function of aperture for both the Circinus galaxy and the measured PSF where used to estimate the size of the emitting region. We find that Circinus is unresolved at 8.6 μm but appears to be marginally extended with a size of $\simeq$ 1.3" (FWHM) at 9.3 μm and 11.3 μm where the s/n is somewhat higher.

3. Quantities derived from the new observations

3.1. Gas and dust mass

The mass of the interstellar medium (ISM) is a crucial quantity for modeling the infrared properties. An estimate of the gas mass can be derived from the dust emission at 1.3mm (Krügel et al., 1990) or from CO line emission; both methods give comparable results (Chini et al., 1992a).

By assuming that the dust emission at 1.3mm is optically thin and that contributions to the 1.3mm flux from sources other than dust emission are negligible the gas mass $M_{gas}^{1.3mm}$ can be estimated from

$$M_{gas}^{1.3mm} = \frac{S_{1.3mm} \cdot D^2}{B_{1.3mm}(T_d) \cdot \kappa_{1.3mm}} \quad (1)$$

where $B(T_d)$ is the Planck function, $S_{1.3mm}$ the observed bolometric flux of the dust emission, and $\kappa_{1.3mm}$ the extinction cross section at 1.3mm. The dust extinction cross section is normalized to cm^2 per gram–ISM in order to derive an estimate of the gas mass.

For a mean dust temperature of T_d = 30 K (Chini et al., 1992b) and an extinction cross section $\kappa_{1.3mm}$ = 0.003 cm^2 per gram–ISM, derived from our standard mixture of carbon and astronomical silicate grains (Chini et al., 1986, Chini et al., 1987, Siebenmorgen & Krügel, 1992), the gas mass $M_{gas}^{1.3mm}$ is about $1.6 \cdot 10^8 M_\odot$.

In this estimate the dust extinction cross section and the assumed gas–to–dust ratio are the least certain quantities (Krügel & Siebenmorgen 1994b; Krügel & Chini 1994). For comparison, if we had assumed that all large grains are made of astronomical silicates, i.e. that no large carbon grains are present in the ISM of the galaxy, then the result would be that $\kappa_{1.3mm} = 7.7 \cdot 10^{-4}$ cm^2 per gram ISM and the derived dust mass would be increased by a factor of 4 accordingly.

We use a "standard" mixture of carbon and astronomical silicate grains and consequently take $M_{gas} = 1.6 \cdot 10^8 M_\odot$ as our best estimate for the gas mass in our models.

3.2. Size of the infrared nuclear source

The size has been best constrained at 3.8μm and 4.8μm where direct imaging gives a FWHM $\leq$ 0.7" and the speckle scans a most probable size of 0.3" or 6 pc. Around 10 μm it is $\simeq$ 1.3" (26pc) and at 20 μm $\leq$ 1.5". Estimates at longer wavelengths are limited by the small sizes and hence large beams of available airborne and space telescopes. At 50 and 100 μm the best size estimate comes from IRAS CPC (Chopped Photometric Channel) observations which reveal a compact source with an estimated but uncertain FWHM $\sim$ 40" and little or no extended emission (Ghosh et al., 1992). Our mm-wave observations give a FWHM $\leq$ 23" at 1.3mm. The source size therefore increases with wavelength but remains smaller than that of the starburst ring up to wavelengths of at least 20 μm.

4. The radiative transfer model

4.1. Model description

In the KS94 model, dust can be heated by i) a central point source, ii) stars in an extended stellar cluster iii) a mean interstellar radiation field and iv) locally in hot spots. These different models of the principle heating sources for the dust are best distinguished by the observed distribution of the IR emission. Hot spot models, which are particularly suited for star-burst galaxies such as M82, show order of magnitude larger mid-IR sizes compared to models having a central point source. In addition to the continuum emission, this model also includes the Si–O stretching vibration at 9.7 μm and the PAH emission features which can be well explained by vibrational excitation of C–H, C=C fundamental modes of polycyclic aromatic hydrocarbons (PAH; Allamandola et al., 1989; Puget & Léger, 1989). Beside the specific resonances of the PAHs, very small dust particles also have to be taken into account since they enhance the near and mid IR emission.

For Circinus, the observations presented here show that at least the mid-infrared luminosity originates in a compact central source which is much smaller than the starburst ring. The photoionization modelling of the high excitation emission lines by M96 and the relative weakness of Brγ in the starburst ring also suggest that re-processed EUV photons from the AGN probably dominate the total infrared luminosity. Our main aim in applying this radiative transfer code, therefore, was to test if a central heating source could adequately reproduce the observed size versus wavelength dependence and overall spectral energy distribution, including the presence of PAH features generally attributed to star forming regions. Having assumed a central power law heating source the remaining 'free' parameters in the model are the:

- **i)** total luminosity (L_{tot}),
- **ii)** slope of power–law AGN component (α),
- **iii)** radius of inner boundary (r_i),
- **iv)** radius of the emitting region (R_{tot}),
- **v)** mass of ISM matter (M_{gas}),
- **vi)** dust density distribution ($\rho(r)$).

These parameters have either been fixed or varied within the observational constraints to achieve the best fit as follows:
i) The intrinsic luminosity of the central source has been assumed equal to the observed total infrared luminosity i.e. $L_{tot} = 1.2 \cdot 10^{10} L_\odot$.
ii) Following M96 we adopt a $\nu^{-0.5}$ spectrum extending from the near infrared to 300 Å below which the dust properties are

unknown (Zubko et al., 1996, Zubko et al., 1997). The resulting infrared spectra are actually relatively insensitive to the exact value in the range $-1 \leq \alpha \leq 1$ and the predicted spectral energy distribution alone cannot be used to definitively distinguish a galactic nucleus powered by a super-massive object from a compact star formation region (Krügel et al., 1983). Both the compact size of the infrared emitting region and the EUV spectrum inferred from the high excitation emission lines, however, argue against a star cluster contributing a significant fraction of the total luminosity.

iii) The inner boundary r_i has been assumed equal to the evaporation temperature (T_{evap}) of the large grains (Churchwell et al., 1990). Since the chemistry of the individual dust populations and other processes involved such as grain sputtering, destruction in shock waves, interaction with charged particles, etc. are not well understood, this parameter is not very precise but sets a lower limit on the inner boundary. We use as evaporation temperature for the silicates $T_{evap}(Si) = 1700K$ and for the large carbon particles T_{evap}(C) = 1200K and find that the grains melt at a distance $r_i \leq 0.25$pc.

iv) We have adopted the upper limit of 23" for the FWHM in our 1.3mm continuum map as the best estimate for the outer radius $R_{tot} \leq 230$pc of the dust emitting region.

v) The adopted gas mass is that deduced from the 1.3mm continuum observations. It depends on the grain properties (see Eq. 1) and is $M_{gas} = 1.6 \cdot 10^8 M_\odot$ for the standard dust model used here.

vi) A resolved far IR or millimeter continuum map is required to derive a good measure of the dust density distribution $\rho(r)$. Here we have assumed that $\rho(r) = \rho_0 \cdot r^{-\beta}$. Both parameters ρ_0 and β are formally constrained by the two conditions required to fit the total gas mass and the depth of the Si–O absorption $\tau_{9.7\mu m}$. Within physically meaningful limits (e.g. $\rho_0 > 0$), we derive for a spherically symmetric dust density distribution:

$$\beta \approx \frac{3c-1}{c-1} \tag{2}$$

where

$$c \approx \frac{M_{gas}}{4\pi R_{tot}^2} \cdot \frac{\kappa_{9.7\mu m}}{\tau_{9.7\mu m}} \tag{3}$$

and

$$\rho_0 \approx \frac{1-\beta}{R_{tot}^{1-\beta}} \cdot \frac{1}{1.4 m_p} \cdot \frac{\tau_{9.7\mu m}}{\kappa_{9.7\mu m}} \tag{4}$$

where m_p denotes the proton mass. The Eq. (2-4), limit the parameter space of the models.

In our standard dust model, we assume spherical dust particles, made of pure carbon or astronomical silicate material and having a power-law size distribution (Mathis et al., 1977). For such a grain mixture and with size parameters as given in Table 2, $\kappa_{9.7\mu m}^{C+Si}$ = 17.6 g/cm^2 is derived. For comparison if one adopts only astronomical silicates for the large grains we find $\kappa_{9.7\mu m}^{Si}$ = 15.5 g/cm^2. Both values of κ are uncertain, as it is known that inhomogeneities, impurities, non-spherically symmetric grain shapes and "fluffiness" have a large influence on the emissivities (Ossenkopf, 1991, 1993, Krügel & Siebenmorgen, 1994b, Stognienko et al., 1995, Siebenmorgen & Gredel, 1997). The depth of the Si-O band was originally estimated by Moorwood & Glass (1984). These authors found $\tau_{9.7\mu m}$ = 1.9 assuming an underlying black-body spectrum with T = 292 K or $\tau_{9.7\mu m}$ = 3.7 assuming an underlying optically thin silicate emission spectrum. We find a slightly better fit to the SED for $\tau_{9.7\mu m}$ = 1.9. Applying parameters as specified in Table 2 into Eq. (2-4) we find $\beta = -0.7$.

4.2. Mathematical formulation

Following the notation by KS94, the radiative transfer equation is written:

$$I(\tau) = I(0) \cdot e^{-\tau} + \int_0^\tau S(x) \cdot e^{-(\tau - x)} dx \tag{5}$$

which is solved for a spherical geometry using a ray tracing method described by Siebenmorgen et al. (1992). The source function $S_\nu(r)$ is

$$S_\nu(r) = \frac{\epsilon_\nu + J_\nu(r) \cdot \kappa_\nu^{\rm sca}}{\kappa_\nu^{\rm ext}} \tag{6}$$

where the dust emission is calculated from

$$\epsilon_\nu = \kappa_\nu^{\rm abs} \int B_\nu(T) P(T) dT \tag{7}$$

Equilibrium temperatures of the large grains are calculated self–consistently for every grain size at every location. The temperature distribution function $P(T)$ accounts for the quantum heating process of the small grains and is computed as discussed by Siebenmorgen et al. (1992). The photo-destruction of the PAHs is calculated as in Siebenmorgen (1993).

The central heating source is introduced by the inner boundary condition:

$$I^+ - I^- = \frac{a}{\pi} \cdot \nu^{-\alpha} \tag{8}$$

where

$$a = \frac{L_{tot}}{4\pi r_i^2} \cdot \begin{cases} \frac{1}{ln(\nu_0/\nu_c)} & \alpha = 0 \\ \frac{1-\alpha}{\nu_0^{1-\alpha} - \nu_c^{1-\alpha}} & \alpha \neq 0 \end{cases} \tag{9}$$

The cut off frequency is not well defined. By using $\nu_c = 4 \cdot 10^{13} Hz$ we ensure that the emission in the IR is due to dust.

5. Model fits

5.1. Observed spectrum

The target overall spectral energy distribution used for testing the models is that shown by Moorwood & Glass (1984) and which comprises ground-based and IRAS photometry and CVF low resolution spectroscopy covering the 3.28μm PAH

and 9.7μm silicate absorption features. Additional CVF spectroscopy of the 3.28μm feature yielded identical fluxes in 7.5 and 10" diameter apertures but a slightly larger equivalent width in the smaller aperture implying that the feature is associated with the nuclear source while the continuum may include some extended stellar contribution (Moorwood, 1986). The recent ISO spectra in a larger aperture of 14 x 20" show a larger 3.28μm equivalent width which may be due to additional PAH emission from the 10" radius starburst ring. The ISO spectra also show prominent 6.2, 7.7, 8.6 and 11.3 μm PAH features which may be associated with the nucleus and/or starburst ring and were not visible in the CVF spectrum due to atmospheric absorption and inadequate spectral sampling.

5.2. Predicted spectrum

The observational constraints on the basic model parameters have already been discussed in Sect. 4. Unless otherwise mentioned, all models have been calculated with a total luminosity L_{tot} = $1.2 \cdot 10^{10}$ $L_\odot$; power law heating source with an index of α = 0.5; distance D = 4Mpc and a gas mass of M_{gas} = $1.6 \cdot 10^8 M_\odot$. Parameters which were varied to investigate their influence on the predicted spectrum are the size of the emitting region, luminosity, gas mass, dust density distribution and the amount and composition of the small grains (PAHs). The best fit parameters are listed in Table 2 and the corresponding predicted SED is shown in Fig. 2 together with the observational data. Agreement between the model and the observations is excellent at all wavelengths except around 100 μm where the small excess flux observed may originate in the starburst region. To test the uniqueness of the fit we have run a large number of models with different parameters.

Small variations of $\simeq$ 20% in R_{tot} have a large effect on the predicted SED because R_{tot} is directly related to the optical depth. The models with an outer shell radius $R \geq R_{tot}$ underestimate the J, H, K colors. By changing the abundance of the silicates with respect to the large carbon grains in our standard model it is possible to improve the near IR fit although such changes are somewhat arbitrary given the information available and the uncertain stellar contribution. One has also to consider that extinction at these wavelengths becomes important so deviations from spherical geometry are no longer negligible (Efstathiou & Rowan-Robinson, 1990). A fully realistic standard Seyfert model would also have to include a torus like structure which requires an axial-symmetric radiative transfer code (Efstathiou & Rowan-Robinson, 1995, Piere & Krolik, 1992). It should be noted that the Si–O absorption is not a good discriminator between star-burst and AGN activity if a spherically symmetric dusty halo is assumed.

Models with constant density distribution (β = 0) show a similarly strong dependence of the SED on R_{tot} and the Si-O absorption. In these models there are more dust grains in the inner cloud regions than for models with $\beta < 0$. More of the large grains are found at higher temperatures and the predicted equivalent widths of the PAH features become too small compared with those observed. Overall the best fit is found for models with β computed using Eq. 2-4.

Table 2. Best fit parameters

Distance	4 Mpc
Luminosity	$1.2 \cdot 10^{10} L_\odot$
Slope of AGN power-law	0.5
Gas mass	$1.6 \cdot 10^8 M_\odot$
Radius of inner boundary	0.25 pc
Radius of dust emission	230 pc
Dust density distribution	$\propto r^{0.7}$
Exponent of dust size distribution	3.5
Lower size of large grains	150 Å
Upper size of large grains	1200 Å
Lower size of small grains	10 Å
Upper size of small grains	80 Å
Abundance* of small grains	0.15
Abundance* of PAH	0.025
Number of C-atoms in PAH	500
H / C atom ratio in PAH	0.1

*Abundance defined relative to solid carbon abundance.

Reducing the total luminosity by e.g. $\simeq$ 30% results in a similar SED shape but lowers the flux by the same factor.

The influence of the gas mass on the SED is shown in Fig. 3. For ease of comparison, all other model parameters are as specified in Table 2. One sees that models with a factor of two higher (lower) gas mass will indeed overestimate (underestimate) the 1.3mm flux by the same and the infrared spectrum by a larger amount. As discussed by Chini et al. (1987), the proportionality, $M_{gas} \propto S_{1.3mm}$, holds as long as the dust temperature is not a strong parameter in Eq. (1). This is the case for cold dust temperatures $\approx$ 30K.

Although the parameters of the small grains are not well constrained we find that large PAH clusters with $\geq$ 300 C atoms provide a good fit. Adopting an extreme cluster abundance of Y_C = 0.25 the total fluxes in the PAH bands are $F(3.28\mu m)$ = 2.3 Jy, $F(6.2\mu m)$ = 14 Jy, $F(7.7\mu m)$ = 13.9 Jy, $F(8.6\mu m)$ = 4.6 Jy and $F(11.3\mu m)$ = 15.4 Jy which are consistent with the ISO SWS spectrum M96. However, after extensive searches in our parameter space we have not found a solution where both the CVF spectra in a small aperture and the ISO SWS in the large aperture can be fit simultaneously. One possible explanation is that the PAH features in the large aperture spectra are dominated by the emission from the starburst ring.

5.3. Sizes

Although the central heating source in our model is a point source the predicted size of the infrared dust emitting region increases with wavelength. Fig. 4 shows the model predictions together with the various observed sizes and upper limits discussed earlier. The best fit model to the SED (solid line) also proves to be consistent with the estimated 10 μm size and the longer wavelength upper limits. It predicts a somewhat larger value than observed at 3 - 5 μm but only by $\simeq$ 60% at 3.8 μm which is probably within the uncertainties. The observed

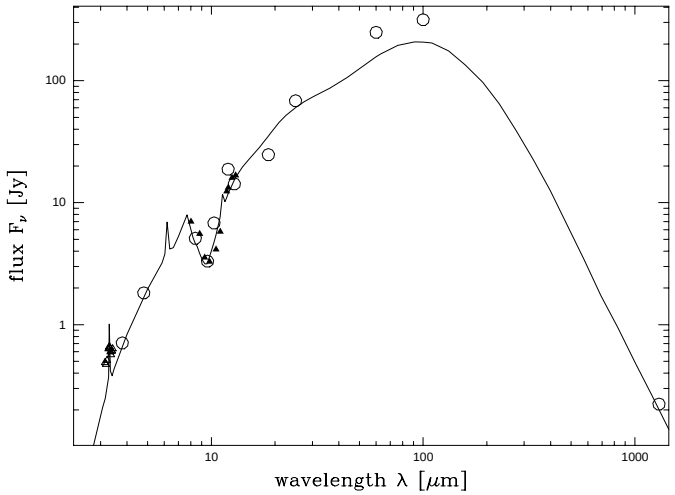

Fig. 2. The SED of the Circinus galaxy. Broad band observations are represented by circles, CVF measurements by triangles and the best fit model (solid line) with parameters as given in Table 2

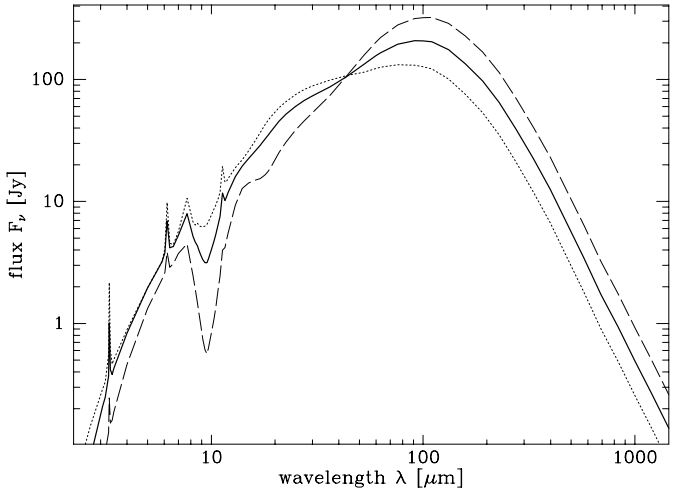

Fig. 3. Influence of the gas mas on the SED of the Circinus galaxy. Results are shown for: $0.5M_{gas}$ (dotted line), M_{gas} (solid line), $2M_{gas}$ (dashed line); other parameters remain as for our standard model (see Table 2).

3.8 μm size of $\sim$ 6pc in fact makes it tempting to identify this emission with the torus proposed in Seyfert unification models (Antonucci, 1993) in which case exact agreement with a spherically symmetrical model cannot be expected.

6. Conclusions

We have presented new observational evidence that the infrared emission from the Circinus galaxy largely originates within a compact region which increases with wavelength but is only a few pc across at 3.8μm, about 26pc around 10μm and still $\leq$ 460 pc at 1.3mm.

Using a spherically symmetric radiative transfer code we have shown that both the observed size versus wavelength and overall spectral energy distribution are consistent with assuming that the infrared emission is mostly from dust heated by the AGN. The many *free* parameters in the model appear to be well constrained by the observations. Although the starburst probably contributes to the $\sim$ 100 μm and PAH emission it is interesting that significant PAH feature emission is predicted by the AGN only model.

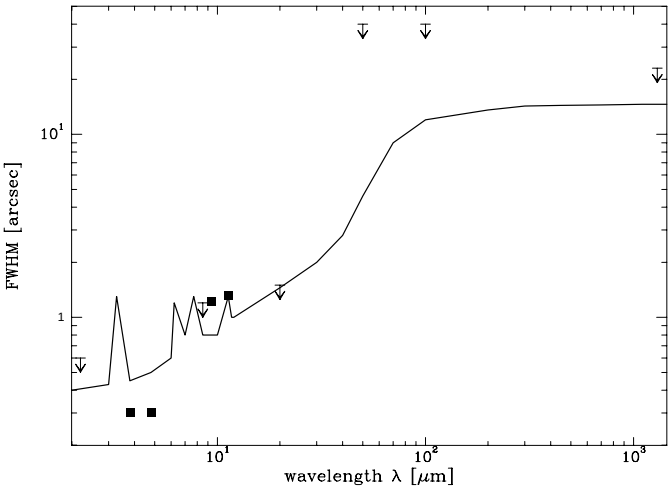

Fig. 4. Size (FWHM) of the emitting region in Circinus as a function of wavelength. The observations are shown as symbols; the solid line represents the model which best fits the SED and whose parameters are given in Table 2.

Acknowledgements. We are grateful to Christian Perrier for making the L and M band speckle observations.

References

Allamandola L.J., Tielens A.G.G.M., Barker J.R., 1989, ApJS, 71, 733.
Antonucci R., 1993, Ann. Rev. Astron. Astrophys., 31, 473.
Chini R., Krügel E., Kreysa E., 1986, A&A 167, 315.
Chini R., Krügel E., Wargau W., 1987, A&A 181, 378.
Chini R., Krügel E., Kreysa E., 1992a, A&A 256, 177
Chini R., Krügel E., Steppe H., 1992b, A&A 255, 87
Churchwell E., Wolfire M.G., Wood D.O.S., 1990, ApJ 354, 247
Efstathiou A., Rowan-Robinson M., 1990, MNRAS 245, 275
Efstathiou A., Rowan-Robinson M., 1995, MNRAS 273, 649.
Freeman C., Karlsson B., Lynga G., et al., 1977, A&A 55, 445.
Ghosh S.K., Bisht R.S., Iyenagar K.V.K., et al., 1992, ApJ, 391, 111.
Hughes D.H., Gear W.K., Robson E.I., 1994, MNRAS 270, 641.
Käufl H.U., Jouan R., Lagage P.O., et al., 1994, Infrared Phys. Technol 35 p 203
Kreysa E., in: From Ground Based to Space-Borne Submm Astronomy, Proc. 29th Liege International Astrophysical Colloquium July, 1990, Longdon N., Kaldeich B. (ed.). ESA SP-314, p. 265
Krügel E., Chini R., 1994, A&A 287, 947.
Krügel E., Siebenmorgen R., 1994, A&A 282, 407 (KS94).
Krügel E., Siebenmorgen R., 1994b, A&A 288, 929.
Krügel E., Chini R., Klein U., et al., 1990, A&A 240, 232.
Krügel E., Tutokov A., Loose H.H., 1983, A&A 124, 89.
Mathis J.S., Rumpl W., Nordsieck K.H., 1977, ApJ 217, 425.
Marconi A., Moorwood A.F.M., Origlia L., Oliva E., 1994, The Messenger, 78. 20.

Matt G., Fiore F., Perola G.C., et al., 1996, MNRAS (in press).
Moorwood A.F.M., 1986, A&A 166, 4
Moorwood A.F.M., Glass I.S., 1984, A&A 135, 281.
Moorwood A.F.M., Oliva E., 1994, Infrared Phys. Tech., 35, 349.
Moorwood A.F.M., Lutz D., Oliva E., et al., 1996, A&A, 315, L109 (M96)
Oliva E., Salvati M., Moorwood A.F.M., Marconi A., 1994, A&A 288, 457.
Ossenkopf V., 1991, A&A 251, 210.
Ossenkopf V., 1993, A&A 280, 617.
Perrier C., 1986, The Messenger, 45, 29.
Puget J.L., Léger A., 1989, ARA&A 27, 161.
Piere E.A., Krolik, J.H., 1992, ApJ 401, 99.
Rowan-Robinson M., Crawford J., 1989, MNRAS 238, 523.
Siebenmorgen R., 1993, ApJ 408, 218.
Siebenmorgen R., Gredel R., 1997, ApJ 485, (in press).
Siebenmorgen R., Krügel E., 1992, A&A 259, 614.
Siebenmorgen R., Krügel E., Mathis J.S., 1992, A&A 266, 501.
Stognienko R., Henning Th., Ossenkopf V., 1995, A&A 296, 797.
Zubko V.G., Mennella V., Colangeli L., Bussoletti E., 1996, in: Käufl H.U. and Siebenmorgen R., "The Role of Dust in the Formation of Stars", ESO, Garching, Germany, September 14, 1995, Springer, Heidelberg.
Zubko V.G., Krelowski J., Wegner W., 1997, MNRAS in press.

This article was processed by the author using Springer-Verlag LaTeX A&A style file *L-AA* version 3.